

Phase separation on surfaces in the presence of matter exchange

Nirvana Caballero ^{1,*}, Karsten Kruse ², and Thierry Giamarchi ¹

¹*Department of Quantum Matter Physics, University of Geneva, 24 Quai Ernest-Ansermet, CH-1211 Geneva, Switzerland*

²*Department of Biochemistry, Department of Theoretical Physics, and NCCR Chemical Biology, University of Geneva, 1211 Geneva, Switzerland*



(Received 6 May 2022; accepted 17 May 2023; published 25 July 2023)

We present a field theory to describe the composition of a surface spontaneously exchanging matter with its bulk environment. By only assuming matter conservation in the system, we show with extensive numerical simulations that, depending on the matter exchange rates, a complex patterned composition distribution emerges on the surface. For one-dimensional systems we show analytically and numerically that coarsening is arrested and as a consequence domains have a characteristic length scale. Our results show that the causes of heterogeneous lipid composition in cellular membranes may be justified in simple physical terms.

DOI: [10.1103/PhysRevE.108.L012801](https://doi.org/10.1103/PhysRevE.108.L012801)

Living cells are full of fluid lipid membranes [1]. The primary function of these membranes is to compartmentalize the cell interior and to separate the cell from its environment. At the same time, diverse patterns that play essential roles in vital processes form on their surfaces. For example, protein clusters acting as units for sensing extra- or intracellular signals [2–5]. These protein clusters can be transient or not and are often associated with domains rich in specific kinds of lipids, commonly designated as lipid rafts [6]. Another spectacular example of membrane-associated patterns are protein waves [7]. Such waves can be standing [8] or traveling [9], which can lead to turbulent dynamics [10]. Some of the surface-associated patterns can be reproduced in reconstitution experiments *in vitro* [11,12].

The physical principles underlying the formation of these patterns are still not fully understood and simple reaction-diffusion systems as pioneered by Turing [13] can miss essential aspects. For example, convective transport along the membrane surface can play an important role [14]. This holds notably for patterns associated with the so-called cytoskeleton, a cellular polymer network in which chemical energy is transformed into mechanical stress [1]. Gradients in this stress lead to flows along the membrane surface [15–17].

Alternatively, in-plane rearrangements in or on a membrane surface can result from phase separation. This is of particular importance for the formation of lipid domains. Lipid phase separation usually results in complete demixing, although the coupling between line tension at the interface between different phases and membrane bending can lead to stable domain patterns [18]. Alternatively, membrane-associated patterns can be formed when the system is kept out of thermodynamic equilibrium [19], for example, through the exchange of matter between the surface and the surrounding medium [20,21] as shown schematically on Fig. 1. Such an

exchange is also essential for the formation of some protein patterns [22].

Pattern formation in the presence of matter exchange between a surface and the surroundings is often studied theoretically using descriptions in which the distribution of particles in the bulk around the surface is assumed *ad hoc* to be homogenous; see for example Refs. [11,20,23]. As a consequence, effective descriptions that only consider the surface are used to analyze the ensuing dynamics. Even though many patterns observed experimentally could be qualitatively reproduced in this way, several observations show that these results have to be considered with care. First, formally the assumption of a homogeneous bulk is not justified. Second, although the patterns may look qualitatively similar to patterns obtained in the full description that also accounts for the bulk, important features may be missed [22,24].

In this work, we consider the case of phase-separating dynamics on a surface in the presence of spontaneous exchange of particles between the surface and the bulk; see Fig. 1. By integrating out the bulk dynamics we obtain an effective model with memory for the time evolution on the surface. We show that the resulting dynamics leads to stationary phase-separated patterns with an intrinsic length scale. We determine this length scale both numerically and via variational arguments. We also compare our results to a previous phenomenological model with a simple instantaneous effective kernel [20]. Our work sheds light on the effects of coupling bulk and surface dynamics for pattern formation.

We consider a surface, which coincides with the plane $z = 0$, such that we neglect surface fluctuations, exchanging matter (from both sides for simplicity) with a bulk. The system is schematized in Fig. 1. We denote by $\vec{r} = (x, y)$ a position on the surface and by $\tilde{m}(\vec{r})$ and $n(\vec{r}, z)$ the densities of particles adhering to the surface and in the bulk respectively. Alternatively, we can interpret \tilde{m} and n as the surface and volume fractions of one component of a two-component system (see Fig. 1), where the two components could be, for example,

*Corresponding author: Nirvana.Caballero@unige.ch

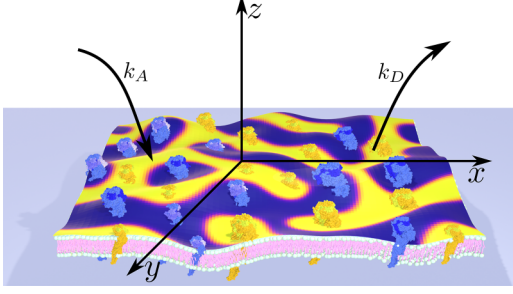


FIG. 1. Illustration of the dynamics considered. Two types of particles (blue and yellow) on a membrane phase, in equilibrium with their respective bulk reservoirs, phase separate into blue and yellow domains. Each species attaches to and detaches from the membrane with the respective rates k_A and k_D .

protein species that can adhere to a membrane or lipid species that constitute the membrane.

Conservation of matter implies that the bulk density $n(\vec{r}, z)$ obeys

$$\partial_t n + \vec{\nabla} \cdot \vec{j} = \delta(z)[k_D \tilde{m}(\vec{r}, t) - k_A n(\vec{r}, z=0, t)], \quad (1)$$

where $\vec{j}(\vec{r}, z, t) = -D\vec{\nabla}n(\vec{r}, z, t)$ is the bulk particle current, which we assume to be purely diffusive with diffusion constant D . Particles close to the membrane attach to the surface at rate k_A , whereas particles on the surface detach at rate k_D . We neglect possible cooperative effects during particle attachment and detachment.

The dynamics of the surface is characterized by either the difference in density of two species $m = \tilde{m}_1 - \tilde{m}_2$ (as shown in Fig. 1) or by the fluctuations of a single species around some average value $m = \tilde{m} - \tilde{m}_0$; see the Supplemental Material (SM) [25]. We consider a Ginzburg-Landau (GL) free energy, symmetric in m , $\mathcal{F} = \int d^2\vec{r} \{ -\frac{\alpha}{2}m^2 + \frac{\delta}{4}m^4 + \frac{\gamma}{2}(\nabla m)^2 \}$ with constants α , β , and γ , to take into account the particles' interactions on the surface. This model is interesting due to the nonlinearity introduced by the GL term. It applies to the single and the two-species case. The applicability is obvious for the single-component case. In the two-species case it applies when the density fluctuations are much smaller than the average density (see the SM). For $\alpha > 0$, it has two minima at $m_{1,2} = \pm\sqrt{\frac{\alpha}{\delta}}$ showing the tendency for phase separation. The dynamics of $m(\vec{r}, t)$ is ruled by a generalized form of the Cahn-Hilliard equation [26,27]:

$$\partial_t m + \vec{\nabla} \cdot \left[-\mu \vec{\nabla} \frac{\delta \mathcal{F}}{\delta m} \right] = k_A n(\vec{r}, z=0, t) - k_D m(\vec{r}, t), \quad (2)$$

where $-\mu \vec{\nabla} \frac{\delta \mathcal{F}}{\delta m}$ is the surface matter current, μ a mobility, and n denotes in this equation either the difference of the two species $n_1 - n_2$ or the density in the bulk shifted by $-\frac{k_D}{k_A}m_0$.

By integrating out the bulk we reduce the two-equations system (1) and (2) to a single equation for $m(\vec{r}, t)$ (see SM [25]):

$$\begin{aligned} \frac{\partial m}{\partial t} &= -\mu \nabla^2 (\alpha m - \delta m^3 + \gamma \nabla^2 m) \\ &+ \int_0^t dt' \int d\vec{r}' K(\vec{r} - \vec{r}', t - t') m(\vec{r}', t'). \end{aligned} \quad (3)$$

The exchanges of matter with the bulk now manifest in this equation as the kernel K

$$\begin{aligned} K(r, t) &= \sqrt{\frac{\pi}{2}} \frac{k_D \kappa}{Dt} e^{-\frac{r^2}{4Dt}} \left(\frac{1}{\sqrt{\pi \kappa t}} - e^{\kappa t} \text{Erfc}(\sqrt{\kappa t}) \right) \\ &- k_D \delta(\vec{r} - \vec{r}') \delta(t - t'), \end{aligned} \quad (4)$$

where $\kappa = \pi \frac{k_A^2}{2D}$.

The kernel is nonlocal in time, representing a memory in the dynamics coming from the diffusion in the bulk. The result (3) is thus a microscopically rooted description of the dynamics of the surface. It must be compared to more phenomenological approaches [20] where the bulk was modeled by a simple *ad hoc* relaxation term, local in space and time,

$$K_\tau = -\tau^{-1} \delta(\vec{r} - \vec{r}') \delta(t - t'), \quad (5)$$

where the parameter τ is a typical matter exchange time. Then, the dynamics is similar to that of phase separating and reacting chemical mixtures [28,29]. We examine below the physical properties of (3) and show that depending on parameters these dynamics, which lead to patterns exhibiting characteristic length scales, they can differ markedly from the phenomenological case.

Because of the kernel memory, solving (3) is much more complicated than for the instantaneous kernel (5). To do so we take advantage of massive parallelization in graphical processing units (GPUs). We consider a system of dimensions $L_x \times L_y$ with $L_x = L_y = 128$ unless stated otherwise and with periodic boundary conditions in both directions. We integrate the dynamical equation by using a semi-implicit Fourier-spectral method [30], adapted from [31,32]. Without loss of generality, we chose $\mu = \alpha = \delta = \gamma = 1$ and space discretization equal to 1. We use D to fix the timescale by choosing $D = 0.1$ and vary k_A and k_D . We approximate the integral in (3) by a Riemann sum that requires the configurations of the system $m(\vec{q}, t)$ in the previous M simulation steps (see SM [25] for more details). For an integration time-step $\Delta t = 10^{-1}$ the difference in $m(\vec{r}, t)$ for simulations with $M = 100$ and $M = 10$ is of the order of 10^{-2} . For our purpose, this is a reasonable numerical error so we fix $\Delta t = 10^{-1}$ and $M = 10$. Typical results obtained from a random initial condition are shown in Fig. 2 together with results for the phenomenological kernel (5) for several values of τ .

In the absence of matter exchange with the bath, $K = 0$, and Eq. (3) reduces to the Cahn-Hilliard equation for which coarsening leads to macroscopic phase separation with eventually two domains of the pure phases m_1 and m_2 . Starting from a random initial condition with $\sum_{\vec{r} \in \text{system}} m(\vec{r}, t) = 0$, we observe macroscopic separation after $\sim 10^5$ simulation steps; see the inset of Fig. 2.

In contrast, in the presence of the full kernel (4) coarsening is interrupted and a natural length scale of the pattern emerges. This can be seen in Fig. 2, where configurations which have evolved from the same random initial condition, but for a much longer time (10^6 steps), exhibit a characteristic pattern. Membrane-bound particles in steady state exhibit a current which vanishes in the absence of matter exchange with the bulk (see SM [25]). To ensure that we were not tricked by slowing down of the dynamics towards complete phase separation, we also considered initial conditions with

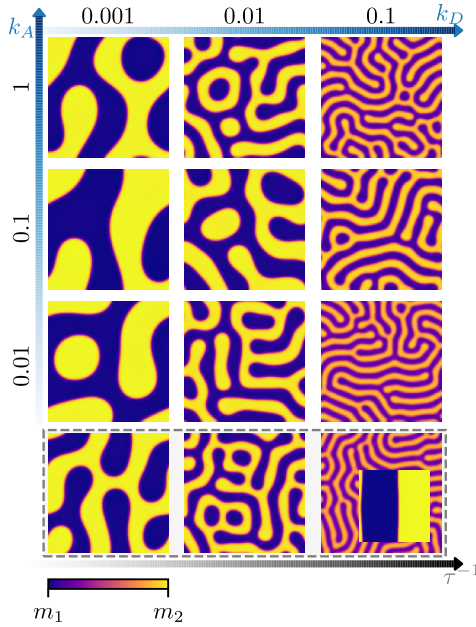


FIG. 2. Snapshots of the distribution m in a domain of 128×128 after 10^6 simulation steps starting from a random initial condition with $\Sigma_{\vec{r} \in \text{system}} m(\vec{r}, t) = 0$. The pure states m_1 and m_2 are given by the minima of the Ginzburg–Landau energy. Top rows 1 to 3: configurations for the full kernel (4). Row 4: configurations for the instantaneous kernel (5). We use $D = 0.1$. The values of the attachment rate k_A , the detachment rate k_D , and the exchange time τ are given in the figure. In the absence of particle exchange with an environment, $K = 0$, the system completely phase separates (inset). In contrast, in the presence of a kernel K coarsening is limited and a natural scale for the patterns appears.

fully separated phases. In the presence of the full kernel (4), stripe or bubble configurations evolved into multiple domains, indicating that patterns with a characteristic length scale are indeed stable fixed points of the dynamics; see SM. In addition to the labyrinthine patterns shown in Fig. 2, which resemble patterns observed in the *Escherichia coli* Min system [33], after a shift in the potential we also found circular patterns (see SM) corresponding to protein or lipid domains frequently found in cells. For simplicity, we continue in the following with the nonshifted potential, but our analysis is readily applicable also in the shifted case.

The steady state patterns exhibit a characteristic length scale determining the width of the meandering stripes. This length scale decreases with increasing detachment rate k_D and shows a nonmonotonic dependence on the attachment rate k_A . In the case of the instantaneous kernel (5) we observe a similar dependence of the characteristic length scale on τ^{-1} . We can estimate the scales of these domains by introducing units to our numerical simulations. For the protein MinD in *E. coli*, the residence time on the membrane was measured *in vitro* to be of the order of 10 s ($k_D^{\text{MinD}} \simeq 10^{-1} \text{ s}^{-1}$) and its diffusion constant D^{MinD} of the order of $10^{-1} \mu\text{m}^2/\text{s}$ [34]. For example, for $k_D = 10^{-2}$ we obtain a timescale $t_0 = \frac{k_D}{k_D^{\text{MinD}}} \simeq 10^{-1} \text{ s}$. Since in our simulations we use $D = 0.1$, this sets the length units to $\xi_0 = \sqrt{\frac{D^{\text{MinD}}}{D}} t_0 \simeq \frac{1}{3} \mu\text{m}$. The attachment rate depends on the cytosolic protein concentration and is more difficult to

get. In particular, there might be cooperative effects, such that the attachment rate can depend on the amount of proteins on the membrane. For MinD *in vitro* a rate $10^{-3} \mu\text{m}/\text{s}$, with a buffer density of $1000 \mu\text{m}^{-3}$, has been previously used in simulations. This gives $k_A \simeq \frac{1}{3} 10^{-3}$. For these values we get domain sizes of approximately $20\xi_0 \simeq 10 \mu\text{m}$, which are of the order of observed domains [33].

In order to rationalize the dependence of the patterns on the matter exchange rates and to quantify the differences between the full and the instantaneous kernels, we first examine the full kernel as a function of momentum and the parameter s resulting from a Laplace transform of the temporal coordinate. In these variables, our kernel (4) reads

$$K(q, s) = -\frac{k_D}{1 + \sqrt{\frac{\kappa}{Dq^2 + s}}}. \quad (6)$$

We see that for small values of the parameter κ , that is small values of the attachment rate k_A or large diffusion constants D , this expression becomes essentially independent of s and thus an instantaneous kernel of the form (5) with the identification $\tau = 1/k_D$. Our microscopic calculation thus validates the use of the instantaneous kernel (5) in such a limit and gives a microscopic value for the effective lifetime τ . In the opposite limit, in contrast, we see that the nonlocal dependence on time has a strong effect on the kernel and we can thus expect different physical behaviors, at least quantitatively.

Let us consider the instantaneous kernel (5) in one spatial dimension. Its dynamics is given by

$$\partial_t m(q, t) = -q^2 \mu \frac{\delta \mathcal{F}_m}{\delta m^*(q, t)}, \quad (7)$$

where the star indicates the complex conjugate, and $q = \frac{2\pi}{L} k$ for a system size L , and $k = 1, \dots, L$. In this expression, we have introduced the pseudo-free energy $\mathcal{F}_m = \mathcal{F} + \mathcal{F}_\tau$, where \mathcal{F} is the GL free energy and \mathcal{F}_τ satisfies

$$\frac{\delta \mathcal{F}_\tau}{\delta m^*(q, t)} = \frac{1}{\tau q^2 \mu} m(q, t). \quad (8)$$

From Eq. (7) it is easy to show that \mathcal{F}_m monotonically decreases under the time evolution and thus that the fixed point of the dynamic evolution must correspond to the minimum of \mathcal{F}_m if it is reachable from the initial configuration. For the parameters of the GL free energy used in this work, we can approximate these states as regions of uniform concentration, where m takes one of the minimal values m_1 or m_2 , separated by narrow transition regions or “kinks.” In the case of the Cahn–Hilliard equation, where $\mathcal{F}_\tau = 0$, these kinks take the form of a hyperbolic tangent, $\sqrt{\frac{\alpha}{2\gamma}} \tanh(\sqrt{\frac{\alpha}{2\gamma}} x)$, and $\mathcal{F} \approx \mathcal{F}_0 + \epsilon_0 n$. Here, n is the (even) number of kinks, ϵ_0 the energy associated with a kink in GL, and \mathcal{F}_0 the energy associated with the uniform regions. The term \mathcal{F}_0 depends only weakly on n . The configuration with minimal energy is thus the one with the minimal number of kinks, i.e., $n = 2$, and corresponds to macroscopic phase separation.

The presence of \mathcal{F}_τ changes this minimum. We can estimate the corresponding number of domains through a variational approach. First, we construct one-dimensional profiles by combining n evenly spaced kinks and probe the

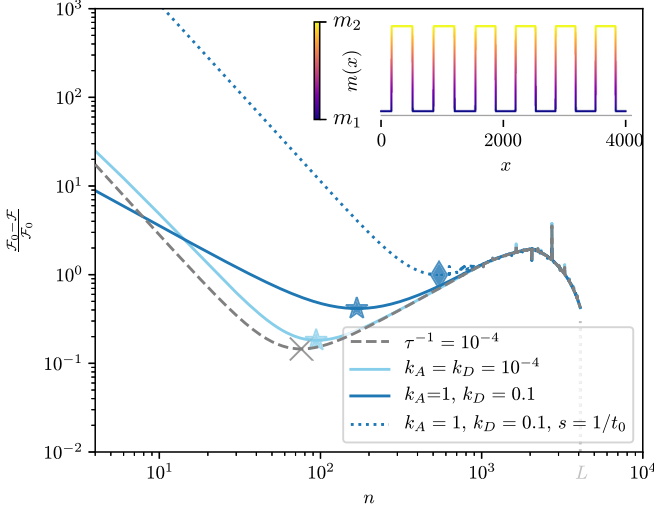


FIG. 3. Pseudo-free-energy \mathcal{F}_m for profiles with n evenly spaced kinks. Dashed line: instantaneous kernel; full lines: full kernel; dotted line: full kernel for $s = 1/t_0 = 1$. Kernel parameters τ^{-1} , k_D , and k_A are as indicated in the legend. The minimum n_{\min} of each energy function is indicated with a symbol. Inset: profile with $n = 12$ kinks.

value of the pseudo-free-energy as a function of n as shown in Fig. 3. For our parameters, kink (and antikink) j with $j = 0, \dots, n/2$ is given by $\theta \tanh(\frac{x-x_j(\theta)}{\sqrt{2}})$, where $\theta = 1$ for $x \in [2jL/n, (2j+1)L/n]$, $\theta = -1$ for $x \in [(2j+1)L/n, 2(j+1)L/n]$, and $x_j(\theta) = (4j+3/2-\theta/2)L/(2n)$. See Fig. 3 inset for an example of the resulting profile. Then, we compute the pseudo-free-energy \mathcal{F}_m for this profile and minimize with respect to n .

Extending this analysis to the case of the full kernel (4) is more involved. A naive attempt could be made from Eq. (6) by assuming that at large times we can approximate this expression by taking $s \rightarrow 0$ and then identifying the resulting q -dependent prefactor with $1/\tau$ in Eq. (8). The pseudo-free-energy has in this case a qualitatively similar shape as for the instantaneous kernel; see Fig. 3.

We test the configurations obtained with the minimization strategy by constructing profiles with n_{\min} number of kinks that serve as initial condition for the full evolution of the dynamic Eq. (3) for both kernels. As shown in Fig. 4(a), the effect of both kernels on the profiles is to slightly distort the shape of the valleys and peaks. As depicted in Fig. 4(b) we see that for the instantaneous kernel the variational solution is essentially stable under time evolution, showing that the variational principle is indeed predicting correctly the fixed point of the dynamics. A simple estimate can be given by noting that \mathcal{F}_τ scales as $L^2 \tau^{-1} n^{-2}$. In the presence of matter exchange in the instantaneous system, we find that the minimum of \mathcal{F}_m is reached for $n = \text{const}(\frac{L^2}{\tau \epsilon_0})^{1/3}$. This scaling relation is in agreement with our numerical results, as shown in Fig. 4(c). However, for the full kernel, the final state differs strongly from the initial configuration derived from the argument above when k_A is large. In particular, the number of kinks is largely different between the variational estimate and the full evolution; see Fig. 4(b). This shows that the naive substitution of the $s = 0$ kernel in the pseudo-free-energy is not sufficient and that a more precise method must be found.

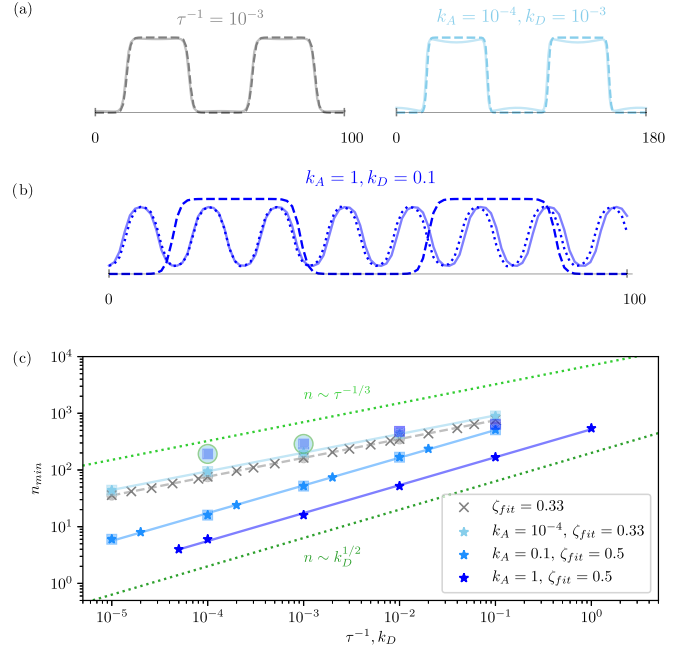


FIG. 4. (a) Part of the profiles used as initial condition (dashed lines) to simulate systems evolving with (5) ($\tau^{-1} = 10^{-4}$) and our kernel (4) for $k_A = 10^{-4}$ and $k_D = \tau^{-1}$. In continuous lines we show the profiles after dynamic evolution. For $k_A = 1$ the number of kinks significantly differs from the number used as initial condition, as shown in (b). For reference in this case we show in dotted lines a constructed profile with the observed n_{\min} and amplitude 0.8. (c) Scaling relation between the optimal number of kinks n_{\min} and the kernel parameters k_D for fixed values of k_A or τ^{-1} depending on the kernel used. Stars and crosses represent respectively for the microscopic and phenomenological kernel an initial condition obtained by minimizing the effective free energy, as shown in Fig. 3. Squares indicate the number of kinks observed in simulations of systems that evolved for up to 10^6 steps from this initial condition and thus correspond up to numerical limitations to the fixed point of the dynamics (the two circles corresponding to $k_A = 1$ and $k_D = 10^{-4}, 10^{-3}$ indicate that the configuration observed for these set of parameters is not regular in contrast with all the other observed configurations). The scaling of n_{\min} appears to be always a power law but with strong quantitative differences between the microscopic and phenomenological kernels as expected when k_A is large. Fits of the data with a power law with exponent ζ_{dis} are shown in dashed and continuous lines for their respective kernels.

Putting phenomenologically a finite s , as shown in Fig. 3, to mimic a finite time cutoff in the memory of the full kernel does push the minimum of the pseudo-free-energy to a larger number of kinks but does not allow for a reliable prediction of the fixed point of the time evolution. Another possibility is that there is more than just one characteristic scale for the domains which could explain why deformed bubble domains were observed in liquid-liquid phase separation of intracellular condensates [35]. Finding the equivalent of a predictive variational approach, if at all possible, for the full kernel is a very interesting but challenging question for future studies. Extension of these methods to the case of the two-dimensional patterns computed numerically in Fig. 2 is also interesting since it would provide direct access to the pattern formation, bypassing the need for the full dynamical analysis.

Beyond the analytical approximations, our simulations show clearly that an optimal length scale exists, revealed by the optimal number of kinks n_{\min} . This number scaling algebraically with the parameters of the kernel. As expected the full and instantaneous kernels essentially coincide at small k_A , whereas largely different behaviors with different exponents are observed when k_A is large; at least for the time available in our simulations. This conveys the importance of having a properly defined full kernel to identify quantitatively the pattern formed.

In this work, we have presented a field theory to describe matter distribution in a membrane exchanging matter with its environment. Our theory predicts arrested phase separation with domains characterized by typical sizes determined by the absorption and expulsion matter exchange rates. Based on semimicroscopical equations for the composition of a surface and its environment, we integrate the environment contribution in a single equation for the surface composition dynamics. The matter exchange effect induces spatiotemporal memory effects with nontrivial consequences for the typical domain sizes for large absorption rates. In contrast, when the absorption rate is low ($k_A \ll 1$) our theory behaves very similarly to an instantaneous kernel that was previously phenomenologically proposed. In this case, we show with semianalytical arguments that matter exchange induces phase separation in the membrane with domains characterized by a typical length. We compute its scaling as a function of the parameters of the problem for the one-dimensional case. Our theory provides a physical justification for the functional form of the instantaneous kernel.

Our theory shows that when the diffusion constant is large or the adsorption rate is low particles detached from the membrane are relatively quickly reabsorbed and homogenized in the bath. The field n describing matter distribution in the environment thus does not play any role and can be neglected in Eq. (2). In this case, the instantaneous kernel can capture the physics of matter exchange on the surface. However, for low diffusion constants or large adsorption rates, the opposite happens and the membrane “remembers” the previous states of the particles. In this case, the instantaneous kernel fails to capture the physics of the problem and the full kernel should be considered. In this case, predicting the domain scaling behavior is more involved and requires further investigation (see the current behavior in the SM [25]).

In future work it will be interesting to study the interplay between phase separation as discussed above and interactions between different lipids and/or proteins induced by membrane undulations. Indeed, such undulations have been argued to induce interactions between transmembrane proteins [36,37] and different lipids in the same [38] or in opposite leaflets of the bilayer membrane [39] and, for large distances, exceed van der Waals or electrostatic forces. As these forces can be attractive or repulsive, we expect a large number of phases to be generated in this case.

This work was supported in part by the Swiss National Science Foundation under Division II (Grant No. 200020-188687). All numerical simulations were performed at the University of Geneva on the *Mafalda* cluster of GPUs.

-
- [1] B. Alberts, A. Johnson, J. Lewis, M. Raff, K. Roberts, and P. Walter, *Molecular Biology of The Cell*, 5th ed. (Garland Science, New York, 2008).
 - [2] J. R. Maddock and L. Shapiro, *Science* **259**, 1717 (1993).
 - [3] R. Varma and S. Mayor, *Nature (London)* **394**, 798 (1998).
 - [4] S. J. Plowman, C. Muncke, R. G. Parton, and J. F. Hancock, *Proc. Natl. Acad. Sci. USA* **102**, 15500 (2005).
 - [5] A. Fujita, J. Cheng, M. Hirakawa, K. Furukawa, S. Kusunoki, and T. Fujimoto, *Mol. Biol. Cell* **18**, 2112 (2007).
 - [6] K. Simons and E. Ikonen, *Nature (London)* **387**, 569 (1997).
 - [7] C. Beta and K. Kruse, *Annu. Rev. Condens. Matter Phys.* **8**, 239 (2017).
 - [8] D. M. Raskin and P. A. J. d. Boer, *Proc. Natl. Acad. Sci. USA* **96**, 4971 (1999).
 - [9] M. G. Vicker, *Biophys. Chem.* **84**, 87 (2000).
 - [10] T. H. Tan, J. Liu, P. W. Miller, M. Tekant, J. Dunkel, and N. Fakhri, *Nat. Phys.* **16**, 657 (2020).
 - [11] M. Loose, E. Fischer-Friedrich, J. Ries, K. Kruse, and P. Schwille, *Science* **320**, 789 (2008).
 - [12] J. Landino, M. Leda, A. Michaud, Z. T. Swider, M. Prom, C. M. Field, W. M. Bement, A. G. Vecchiarelli, A. B. Goryachev, and A. L. Miller, *Curr. Biol.* **31**, P5613 (2021).
 - [13] A. M. Turing, *Phil. Trans. R. Soc. B* **237**, 37 (1952).
 - [14] J. Fan, M. Sammalkorpi, and M. Haataja, *Phys. Rev. Lett.* **100**, 178102 (2008).
 - [15] J. S. Bois, F. Jülicher, and S. W. Grill, *Phys. Rev. Lett.* **106**, 028103 (2011).
 - [16] K. V. Kumar, J. S. Bois, F. Jülicher, and S. W. Grill, *Phys. Rev. Lett.* **112**, 208101 (2014).
 - [17] E. Hannezo, B. Dong, P. Recho, J.-F. Joanny, and S. Hayashi, *Proc. Natl. Acad. Sci. USA* **112**, 8620 (2015).
 - [18] T. Baumgart, S. T. Hess, and W. W. Webb, *Nature (London)* **425**, 821 (2003).
 - [19] X. Fang, K. Kruse, T. Lu, and J. Wang, *Rev. Mod. Phys.* **91**, 045004 (2019).
 - [20] L. Foret, *Europhys. Lett.* **71**, 508 (2005).
 - [21] M. S. Turner, P. Sens, and N. D. Socci, *Phys. Rev. Lett.* **95**, 168301 (2005).
 - [22] L. Wettmann and K. Kruse, *Phil. Trans. R. Soc. B* **373**, 20170111 (2018).
 - [23] W. M. Bement, M. Leda, A. M. Moe, A. M. Kita, M. E. Larson, A. E. Golding, C. Pfeuti, K.-C. Su, A. L. Miller, A. B. Goryachev, and G. v. Dassow, *Nat. Cell Biol.* **17**, 1471 (2015).
 - [24] N. Levernier and K. Kruse, *New J. Phys.* **22**, 013003 (2020).
 - [25] See Supplemental Material at <http://link.aps.org/supplemental/10.1103/PhysRevE.108.L012801> for a comprehensive explanation of how our model can describe matter distributions of one or two components, including Ref. [40].
 - [26] P. M. Chaikin, T. C. Lubensky, and T. A. Witten, *Principles of Condensed Matter Physics* (Cambridge University Press, Cambridge, 1995), Vol. 10.
 - [27] L. F. Cugliandolo, *C. R. Phys.* **16**, 257 (2015).
 - [28] B. A. Huberman, *J. Chem. Phys.* **65**, 2013 (1976).

- [29] S. C. Glotzer, E. A. Di Marzio, and M. Muthukumar, *Phys. Rev. Lett.* **74**, 2034 (1995).
- [30] L. Q. Chen and J. Shen, *Comput. Phys. Commun.* **108**, 147 (1998).
- [31] N. B. Caballero, E. E. Ferrero, A. B. Kolton, J. Curiale, V. Jeudy, and S. Bustingorry, *Phys. Rev. E* **97**, 062122 (2018).
- [32] N. Caballero, *J. Stat. Mech.* (2021) 103207.
- [33] P. Glock, B. Ramm, T. Heermann, S. Kretschmer, J. Schweizer, J. Mücksch, G. Alagöz, and P. Schwille, *ACS Synth. Biol.* **8**, 148 (2019).
- [34] M. Loose, E. Fischer-Friedrich, C. Herold, K. Kruse, and P. Schwille, *Nat. Struc. Mol. Biol.* **18**, 577 (2011).
- [35] J. A. Riback, L. Zhu, M. C. Ferrolino, M. Tolbert, D. M. Mitrea, D. W. Sanders, M.-T. Wei, R. W. Kriwacki, and C. P. Brangwynne, *Nature (London)* **581**, 209 (2020).
- [36] M. Goulian, R. Bruinsma, and P. Pincus, *Europhys. Lett.* **22**, 145 (1993).
- [37] J.-M. Park and T. Lubensky, *J. Phys. I France* **6**, 1217 (1996).
- [38] D. S. Dean, V. A. Parsegian, and R. Podgornika, *J. Phys.: Condens. Matter* **27**, 214004 (2015).
- [39] M. P. Haataja, *Biophys. J.* **112**, 655 (2017).
- [40] R. P. Feynman, *Statistical Mechanics: A Set of Lectures* (CRC, Boca Raton, 2018).